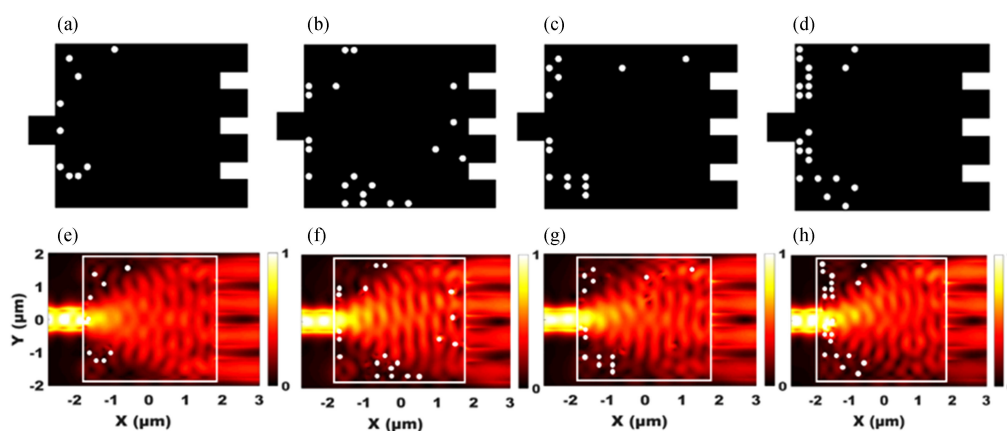


Inversely Designed 1×4 Power Splitter With Arbitrary Ratios at $2\text{-}\mu\text{m}$ Spectral Band




Volume 10, Number 4, August 2018

Hucheng Xie
Yingjie Liu
Wenzhao Sun
Yujie Wang
Ke Xu, *Member, IEEE*
Jiangbing Du, *Member, IEEE*
Zuyuan He, *Senior Member, IEEE*
Qinghai Song



DOI: 10.1109/JPHOT.2018.2863122
1943-0655 © 2018 IEEE

Inversely Designed 1×4 Power Splitter With Arbitrary Ratios at $2\text{-}\mu\text{m}$ Spectral Band

Hucheng Xie,¹ Yingjie Liu,¹ Wenzhao Sun,¹ Yujie Wang,¹
 Ke Xu ¹, Member, IEEE, Jiangbing Du ², Member, IEEE,
 Zuyuan He ², Senior Member, IEEE, and Qinghai Song¹

¹Harbin Institute of Technology (Shenzhen), Shenzhen 518055, China

²State Key Laboratory of Advanced Optical Communication Systems and Networks,
 Shanghai Jiao Tong University, Shanghai 200240, China

DOI:10.1109/JPHOT.2018.2863122

1943-0655 © 2018 IEEE. Translations and content mining are permitted for academic research only.

Personal use is also permitted, but republication/redistribution requires IEEE permission.

See http://www.ieee.org/publications_standards/publications/rights/index.html for more information.

Manuscript received May 28, 2018; revised July 27, 2018; accepted August 1, 2018. Date of publication July 16, 2018; date of current version August 15, 2018. National Natural Science Foundation of China (NSFC) (61505039, 61675128, 61775138). Shenzhen Fundamental research projects (JCYJ20170307151047646) and Open Fund of IPOC 2016B005. Corresponding authors: Ke Xu and Jiangbing Du (e-mail: kxu@hit.edu.cn; dujiangbing@sjtu.edu.cn).

Abstract: We demonstrate integrated 1×4 power splitters at $2\text{-}\mu\text{m}$ spectral range with arbitrary power-splitting ratios. The devices are based on digital meta-structures that are designed by algorithm. Four devices with split ratios of 1:1:1:1, 2:2:1:1, 2:2:2:1, and 4:3:2:1 are inversely designed to conceptually prove the capability of arbitrary split ratios. Up to four design objectives including both efficiency and power ratios between the four outputs of each device have been jointly optimized. The total transmission efficiencies of all the algorithm-optimized splitters are above 80%, which is predicted by simulations. The power ratios are well consistent with the design targets as well. Then, the devices are fabricated on silicon-on-insulator platform with the device footprint of only $3.6 \mu\text{m} \times 3.6 \mu\text{m}$. The fabricated splitters are characterized at wavelength range from 1945 to 1975 nm. The total transmission efficiencies of all the splitters are measured to be higher than 70%, and the power ratios agree with the simulation results.

Index Terms: Inverse design, Multi-port power splitter with arbitrary ratios.

1. Introduction

Multimode interferometer (MMI) is one of the fundamental building blocks in photonic integrated circuits. The self-imaging properties enable the MMI to be an excellent candidate for optical power splitter with small footprint and large number of port counts. By reproducing multiple images of the input field along the wave propagation, the power is equally divided in the multimode waveguide region. Apparently, power splitter with design freedom for arbitrary power ratio is more attractive as it will have much wider scope of applications such as feedback circuits, tap-port power monitoring, power-equalized or power-imbalanced beam splitting circuits and so on. While regular MMI is hardly able to achieve unequal power split, several sophisticated designs are proposed to demonstrate the splitter with variable ratios [1]–[5]. It can be noticed that most of these techniques are demonstrated for splitter with only two output ports. This is due to the exponentially increasing design difficulties with more port counts.

Inverse design with digital or free-form meta-structure were recently demonstrated with powerful design capability [6]–[11]. Such meta-structures enable much larger parameter spaces compared with regular device structures that is designed by manually tuning a limited number of parameters. Inverse design promise incredibly large design freedom by using algorithm to handle the numerous structural parameters. Ratio-flexible power splitter has been realized by L. Liu *et al.* with three output ports for the first time [12]. A broadband 3-way power divider was also reported using a free-form device topology in [13]. A common feature of such inverse design methods is setting the objective first and iteratively optimize the structure towards the design target. Though many devices with unprecedented functionalities or superior performance have been reported based on inverse design, there were few demonstrations of complex functional devices with more than three design objectives.

In this paper, we investigate a four-objective design problem and demonstrate an ultra-compact 1×4 power splitter with arbitrary ratios. The device transmission efficiency and the power ratios between the four output ports are jointly optimized by algorithm. Splitters with four different power ratios are designed at $2\text{-}\mu\text{m}$ spectral band which has been recently proposed to be a promising window for optical communications and on-chip applications [14]–[17]. Besides, compared with the $1.55\text{-}\mu\text{m}$ devices, the required pixel dimension is larger which improves the fabrication tolerance. The devices are fabricated on silicon-on-insulator (SOI) and the characterization results are well consistent with the theoretical predictions.

2. Design Method

The devices are designed on the SOI platform with $2\text{-}\mu\text{m}$ buried oxide (BOX) and 220 nm top silicon. The optical wave is manipulated in an MMI area with a size of $3.6\text{ }\mu\text{m} \times 3.6\text{ }\mu\text{m}$. The waveguides in this work are all fully etched to the BOX layer. Initially, the MMI structure is discretized with 18×18 pixels. Each pixel is a circular shape nanohole with diameter of 140 nm , which can be easily fabricated by E-beam lithography in our clean room. It can also be possibly fabricated using the silicon etching step in $0.13\text{ }\mu\text{m}$ CMOS process in the commercial foundry. Even though the pixel dimension is chosen to be larger than that in [12], the wavelength to pixel-dimension ratio is not reduced. Compared with the previously demonstrated QR code like structure [12], the circular shape nanoholes are more tolerant to fabrication error compared to square shape [11]. These pixels have a binary state of material property: silicon or air. It allows for nearly free-form refractive index engineering by choosing the appropriate index of these pixels. We consider the fundamental transverse electric (TE) mode and wavelength from 1940 nm to 1980 nm as the input light source in the simulations. Though some of the inversely-design functionalities are highly dependent on the initial discretized structure, we just launch the optimization from an all-silicon MMI structure without defining the initial structure specifically. The optimization is performed via direct binary search method that has been demonstrated for various devices [7], [8]. But none of the previous demonstrations have handled more than 3 objectives during the optimization according to our best knowledge. For 1×4 power splitter with arbitrary ratios, the structural parameters are optimized by the following procedure.

In this case, there are two principal figures-of-merits (FOMs): one is the total transmission efficiency of all the output ports, which can be described as $\sum_{i=1}^4 E_i$ where E_i is the efficiency of the i -th output port ($i = 1, 2, 3, 4$). The other FOMs are the power ratios between each output port. which can be expressed as E_1/E_4 , E_2/E_4 , E_3/E_4 . Hence, there are 4 FOMs needs to be optimized. The efficiencies of all the outputs can be numerically calculated by 3D fine difference time domain (FDTD) method. While it is too complicated to optimize all the FOMs in parallel, we treat the transmission efficiency as the first-priority target. Thus, we set the first-step conditions of convergence as:

$$\left(\frac{\sum_{i=1}^4 E_{i,j+1}}{\sum_{i=1}^4 E_{i,j}} > 1 \right) \bigcap_{i=1}^3 \left[\left(\frac{E_{i,j+1}}{E_{4,j+1}} - \alpha_i \right)^2 < \rho_{i,j+1}^2 \right] \quad (1)$$

where $E_{i,j}$ and α_i stand for the transmission efficiency of i -th port in the j -th iteration and the desired power split ratio. $\rho_{i,j+1}$ is the radius of convergence for i -th port in the $(j + 1)$ th iteration and dynamically varies according to the feedback. In this step, the total efficiency of the device is forced to improve after each iteration while the split ratio is maintained within a certain range. The radius of convergence $\rho_{i,j}$ could be expressed as:

$$\alpha_{i,j} = f_i \left(\sum_{i=1}^4 E_{i,j} \right) \quad (2)$$

It should be noted that $f_i(x)$ is a decreasing function which comes to zero after a certain number of iterations. An optimization with a fast-convergent rate normally requires strong convexity of objective [18]. In our design, a parabolic function is set as $f_i(x)$ to approximate the radius of convergence in the whole process of optimization. In this step, the efficiency can be quickly optimized to 80% as the efficiency increase is a hard decision in eqn. (1).

The second step is the optimization of power split ratios when the total transmission efficiency reaches to 80%. The optimization condition could also be described as:

$$\left[\frac{\left(\frac{E_{1,j+1}}{E_{4,j+1}} - \alpha_1 \right)^2}{\left(\frac{E_{1,j}}{E_{4,j}} - \alpha_1 \right)^2} < 1 \right] \bigcap_{k=i+1}^3 \left[\left(\frac{E_{k,j+1}}{E_{4,j+1}} - \alpha_k \right)^2 < \rho_{k,j+1}^2 \right] (i = 1, 2, 3) \quad (3)$$

We first optimize the power split ratio of E_1/E_4 which is the ratio between Port 1 and Port 4. The $(j + 1)$ -th iteration result is effective only if the value of $\left(\frac{E_{1,j+1}}{E_{4,j+1}} - \alpha_1 \right)^2$ in $(j + 1)$ -th iteration which representing the power ratio discrepancy is reduced. Due to such a hard requirement, the ratio between Port1 and Port4 are forced to getting close to the designed ratio. In the meantime, the other two power ratios E_2/E_4 , E_3/E_4 are controlled within a certain range by the radius of convergent $\rho_{k,j+1}$. The optimization of E_1/E_4 is completed when the value of $\left(\frac{E_{1,j+1}}{E_{4,j+1}} - \alpha_1 \right)^2$ is smaller than a threshold value. The power ratios of E_2/E_4 and E_3/E_4 could also be optimized by the similar procedure.

3. Results and Discussions

We use a 4-core desktop computer operating at 3.4 GHz to perform the optimization, and the computation cost is within 48hrs in average for each device. To demonstrate the ability of arbitrarily splitting the optical power, we investigate four different cases with the power ratios of: 1:1:1:1, 1:1:2:2, 2:2:2:1, 4:3:2:1. Upon the completion of the optimization process, we got a set of structures that split the optical power with the desired ratios. The schematic diagrams of the designed device structures are shown in Fig. 1(a)–(d). The circular pixels represent the air holes where the silicon is etched away. It should be noted that, only a few air pixels are needed and are located in the region where very little field is present, which is quite different to the previous QR-code-like functional devices with a large number of etched holes. This is because the initial structure is coincidentally quite close to a perfect 1×4 MMI splitter and thus there is no need to induce too many index-engineered unit cells for beam steering. Even though only a few pixels are etched away, they do have a significant impact on the optical wave propagation through the multimode waveguide region. Fig. 1(e)–(f) are the corresponding optical fields distributions at 1950 nm wavelength that were obtained via 3D FDTD simulations. With the same size of the multimode region, the different power ratios are observed at the output which is due to the beam steering effect induced by the air holes. Though the air holes inevitably induce some scattering loss, the numerically calculated transmittance of all the output ports exceeds 80% for all the cases: 83%, 82%, 82% and 80% for the power ratios of 1:1:1:1, 1:1:2:2, 2:2:2:1 and 4:3:2:1, respectively. Such devices can operate over a wide wavelength range in 2- μ m band as indicated by the simulated spectral responses of the power split ratios shown in Fig. 2(a)–(d). The results indicate that for all the cases, the split ratios are well consistent with the design targets within the spectral range from 1940–1980 nm. Since the

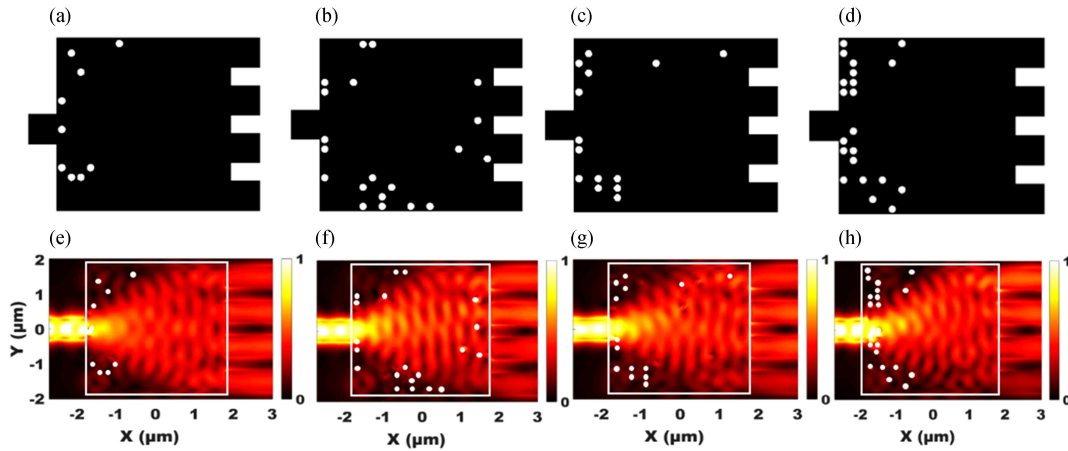


Fig. 1. (a)–(d) The schematic picture of optimized structures of ratio: (a) split ratio of 1:1:1:1. (b) split ratio of 2:2:1:1. (c) split ratio of 2:2:2:1. (d) split ratio of 4:3:2:1. (e)–(h) The numerically calculated electric fields for four optimized structures corresponding to the structures in (a)–(d), respectively.

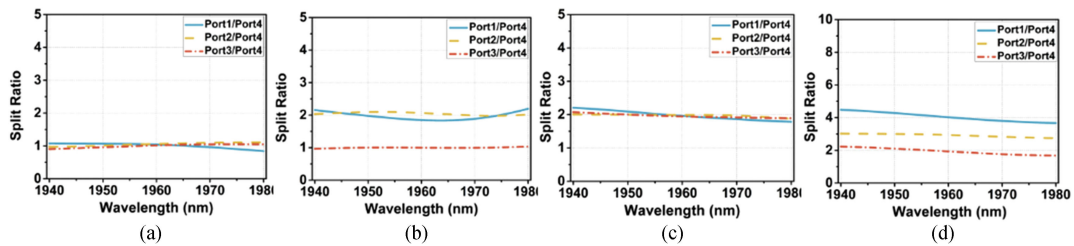


Fig. 2. (a)–(d) Simulated power split ratios of four structures: (a) split ratio of 1:1:1:1. (b) split ratio of 2:2:1:1. (c) split ratio of 2:2:2:1. (d) split ratio of 4:3:2:1.

optimization process is highly dependent on the initial structure, we may try different initial structure which might get us higher efficiencies. Increasing the optimization time or trying different algorithm also help to improve the efficiency. Another method is to increase the number of pixel while it will increase the device footprint and computation cost.

Due to the fabrication imperfection, fabricating the nanoholes with exactly the designed dimensions is challenging. Though the circular shape pixels are easier to fabricate than the square pixels which have too many sharp corners, it is rather difficult to control the hole size. In order to investigate the fabrication tolerance of these nanostructured splitters, we run the simulations with all the parameters unchanged except for the radii of nanoholes. Here, we define the normalized FOM error as $|1 - \frac{E_i/E_d}{\alpha_i}|$ ($i = 1, 2, 3$) which could be used to approximate the deviation between the simulated value and desired value. Then, we study the fabrication error induced performance degradation with the pixel diameters varies from -30 nm to 30 nm. These variations in nanohole diameter result in FOM errors which are numerically calculated and plotted in Fig. 3(a)–(d). It could be found obviously that the FOM error become larger with the increased diameter variations for all the devices. We can also find that the device with split ratio of 4:3:2:1 is much more sensitive to the diameter variations. The possible reason is that this device has more air pixels compared to other three devices. In general, the simulated results suggest that these devices are relatively tolerant to fabrication error under ± 10 nm variation of diameter.

4. Fabrication and Measurement

The designed meta-structure-based optical splitters with different ratios are fabricated on SOI wafer (SOITEC, Inc.) with $2\ \mu\text{m}$ BOX and $220\ \text{nm}$ top silicon. The positive resist ZEP 520A is spin coated

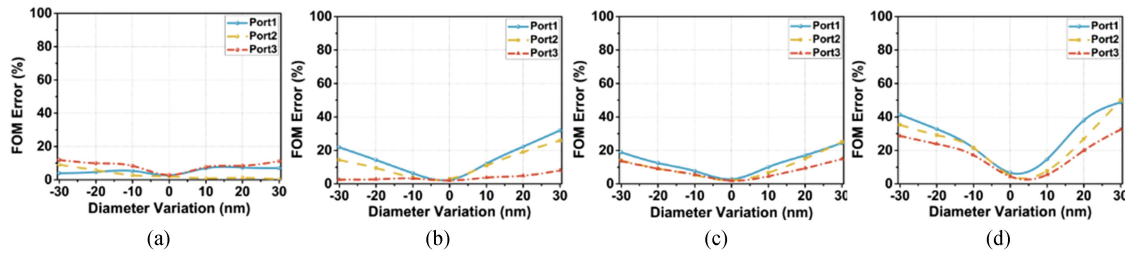


Fig. 3. (a)–(d) Simulated FOM error of four structures: (a) split ratio of 1:1:1:1. (b) split ratio of 2:2:1:1. (c) split ratio of 2:2:2:1. (d) split ratio of 4:3:2:1.

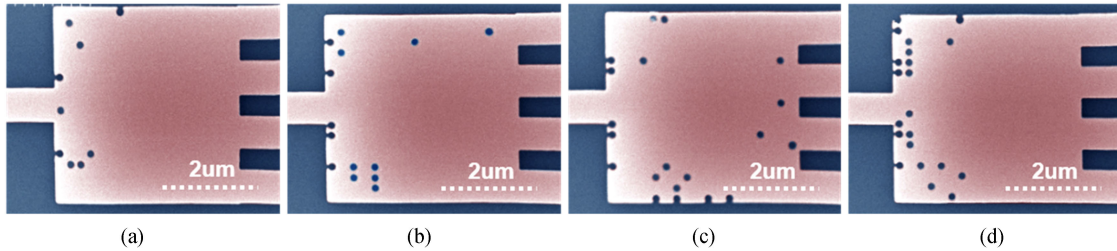


Fig. 4. The SEM images of four optimized structures: (a) split ratio of 1:1:1:1. (b) split ratio of 2:2:1:1. (c) split ratio of 2:2:2:1. (d) split ratio of 4:3:2:1.

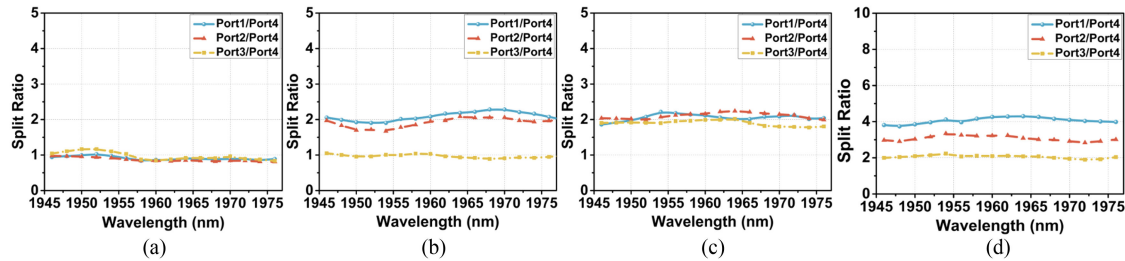


Fig. 5. (a)–(d) Measured power split ratios of four structures: (a) split ratio of 1:1:1:1. (b) split ratio of 2:2:1:1. (c) split ratio of 2:2:2:1. (d) split ratio of 4:3:2:1.

on the silicon chip before the device layout is patterned by electron beam lithography which operates at 30 kV (Raith eLINE). Then inductively coupled plasma (ICP) is used to etch the silicon and remove the residual photo resist after the pattern is transferred onto the silicon layer. The top-view scanning electron microscope (SEM) pictures of the fabricated devices with different split ratios are shown in Fig. 4(a)–(d). The air holes are well etched and located as we designed. The average diameter of these pixels is measured to be 136 nm which is very close to the design value. According to the fabrication tolerance investigation shown in Fig. 3, these errors will have negligible impact on the experimental results.

The devices are measured by a continuous wave tunable laser operate at $2\text{-}\mu\text{m}$ waveband. The polarization of the laser output is aligned by a hand-made three-paddle polarization controller. Then, the light is coupled into the silicon waveguide via a fully-etched grating coupler with 10° off-normal tilt. Another grating coupler is used for coupling out the optical signal to a power meter. We scan the laser wavelength in a step mode and normalize the measured optical power by subtracting the coupling loss which is characterized by a pair of reference grating coupler. The power split ratios E_1/E_4 , E_2/E_4 , E_3/E_4 of all the four devices are plotted in Fig. 5(a)–(d). The experimental results match the simulation results quite well. Due to the limited spectral range of the laser emission, we measured power ratios for all the devices from 1945–1980 nm with a wavelength step size of 2 nm. The measured total transmission efficiencies are 77%, 73%, 75% and 71% for the power

ratios of 1:1:1:1, 1:1:2:2, 2:2:2:1 and 4:3:2:1, respectively, which are a bit lower than the simulated value. The possible reason for the additional loss is the additional scattering induced by fabrication imperfection like side wall roughness. It can be seen that the ratios between different outputs are quite close to the target values over this wavelength range.

5. Conclusion

In summary, we have demonstrated 1×4 optical power splitter with four different power split ratios: 1:1:1:1, 2:2:1:1, 2:2:2:1 and 4:3:2:1. The devices are based on digital waveguide meta-structures and are inversely designed by algorithm. Four objectives are jointly optimized and convergent results are obtained within 48 hours in average. The splitters have compact footprint of only $3.6 \mu\text{m} \times 3.6 \mu\text{m}$ and operate at $2\text{-}\mu\text{m}$ waveband. The long waveband allows for a larger pixel dimension of 140 nm compared with the previous demonstrations of inversely designed devices at C band. The measured total efficiency and the power ratios between the output ports agree well with the theoretical simulations. In principle, arbitrary split ratios and more channels can be achieved by the joint optimization method discussed in this work.

References

- [1] Q. Deng, L. Liu, X. Li, and Z. Zhou, "Arbitrary-ratio 1×2 power splitter based on asymmetric multimode interference," *Opt. Lett.*, vol. 39, no. 19, pp. 5590–5593, 2014.
- [2] D. Levy, Y. Li, R. Scarmozzino, and R. M. Osgood, "A multimode interference-based variable power splitter in GaAs–AlGaAs," *IEEE Photon. Technol. Lett.*, vol. 9, no. 10, pp. 1373–1375, Oct. 1997.
- [3] J. Leuthold and C. H. Joyner, "Multimode interference couplers with tunable power splitting ratios," *J. Lightw. Technol.*, vol. 19, no. 5, pp. 700–707, May 2001.
- [4] X. Deng, L. Yan, H. Jiang, W. Pan, B. Luo, and X. Zou, "Polarization-insensitive and broadband optical power splitter with a tunable power splitting ratio," *IEEE Photon. J.*, vol. 9, no. 3, Jun. 2017, Art. no. 4501609.
- [5] Y. Tian *et al.*, "Broadband 1×3 couplers with variable splitting ratio using cascaded step-size MMI," *IEEE Photon. J.*, vol. 10, no. 3, Jun. 2018, Art. no. 6601008.
- [6] A. Y. Piggott, J. Lu, K. G. Lagoudakis, J. Petykiewicz, T. M. Babinec, and J. Vuckovic, "Inverse design and demonstration of a compact and broadband on-chip wavelength demultiplexer," *Nature Photon.*, vol. 9, pp. 374–377, 2015.
- [7] B. Shen, P. Wang, R. Polson, and R. Menon, "An integrated-nanophotonics polarization beamsplitter with $2.4 \times 2.4 \mu\text{m}^2$ footprint," *Nature Photon.*, vol. 9, pp. 378–382, 2015.
- [8] Y. Liu *et al.*, "Very sharp adiabatic bends based on an inverse design," *Opt. Lett.*, vol. 43, no. 11, pp. 2482–2485, 2018.
- [9] Z. Yu, H. Cui, and X. K. Sun, "Genetic-algorithm-optimized wideband on-chip polarization rotator with an ultrasmall footprint," *Opt. Lett.*, vol. 42, no. 16, pp. 3093–3096, 2017.
- [10] J. C. C. Mak, C. Sideris, J. Jeong, A. Hahimiri, and J. K. S. Poon, "Binary particle swarm optimized 2×2 power splitters in a standard foundry silicon photonic platform," *Opt. Lett.*, vol. 41, no. 16, pp. 3868–3871, 2016.
- [11] W. Chang *et al.*, "Ultra-compact mode (de) multiplexer based on subwavelength asymmetric Y-junction," *Opt. Exp.*, vol. 26, no. 7, pp. 8162–8170, 2018.
- [12] K. Xu *et al.*, "Integrated photonic power divider with arbitrary power ratios," *Opt. Lett.*, vol. 42, no. 4, pp. 855–858, 2017.
- [13] A. Y. Piggott, J. Petykiewicz, L. Su, and J. Vuckovic, "Fabrication-constrained nanophotonic inverse design," *Sci. Rep.*, vol. 7, 2017, Art. no. 1786.
- [14] J. J. Ackert *et al.*, "High-speed detection at two micrometres with monolithic silicon photodiodes," *Nat. Photon.*, vol. 9, no. 10, pp. 393–396, 2015.
- [15] J. Li *et al.*, " $2\text{-}\mu\text{m}$ wavelength grating coupler, bent waveguide, and tunable microring on silicon photonic MPW," *IEEE Photon. Technol. Lett.*, vol. 30, no. 5, pp. 471–474, Mar. 2018.
- [16] K. Xu, L. Sun, Y. Q. Xie, Q. Song, J. B. Du, and Z. He, "Transmission of IM/DD signals at $2 \mu\text{m}$ wavelength using PAM and CAP," *IEEE Photon. J.*, vol. 8, no. 5, Oct. 2016, Art. no. 7906407.
- [17] H. Zhang *et al.*, "Dense WDM transmission at $2 \mu\text{m}$ enabled by an arrayed waveguide grating," *Opt. Lett.*, vol. 40, no. 14, pp. 3308–3311, 2015.
- [18] D. Garber and E. Hazan, "Faster rates for the frank-wolfe method over strongly-convex sets," in *Proc. 32nd Int. Conf. Machine Learning* 2015, vol. 37, pp. 541–549.